Eocene biostratigraphy and magnetic stratigraphy from Possagno, Italy: The calcareous nannofossil response to climate variability

Claudia Agnini [a,*], Giovanni Muttoni [b,c], Dennis V. Kent [d,e], Domenico Rio [a]

[a] Department of Geology, Paleontology and Geophysics, University of Padova, Via Giotto, 1 I-35137 Padova, Italy
[b] Department of Earth Sciences, University of Milan, Via Mangiagalli 34, I-20133 Milan, Italy
[c] ALP—Alpine Laboratory of Paleomagnetism, via Madonna dei Boschi 76, I-12016 Peveragno (CN), Italy
[d] Department of Geological Sciences, Rutgers University, Piscataway, NJ 08854, U.S.A.
[e] Lamont-Doherty Earth Observatory, Palisades, NY 10964, U.S.A.

Abstract

A study of quantitative calcareous nannofossil biostratigraphy and magnetostratigraphy of a ~68-m-thick marine limestone section of Late Paleocene–Middle Eocene age outcropping at Possagno in northern Italy shows that the section encompasses nannofossil Zones NP9–NP15 (equivalent to CP8–CP13b) and Chrons C24r–C21n. The Paleocene–Eocene boundary was placed at the base a of $\delta^{13}C$ negative excursion from the literature that was found virtually coincident with the base of Zone NP9b. The base of the Middle Eocene (Lutetian) was placed at the base of Chron C21r. Biostratigraphic events were generally found to be consistent with parallel events in recent time scales; several potentially useful new events are also described. In particular, we detected the earliest specimens of *Dictyococcites* at the base of Chron C22r (NP12–NP13 zonal transition), which is several million years older than previous estimates. Correlation of Possagno data to the oxygen isotope record from the literature allowed us to describe the temporal relationships between climate variability and calcareous nannofossil assemblages. Modifications in the nannofossil assemblage coeval to both the Paleocene–Eocene Thermal Maximum (PETM) and the Early–Middle Eocene long-term climatic trend are recognized. The short-lived PETM was coeval to provisional adaptations (malformations and/or ecophenotypes) in the coccolithophores communities that were reabsorbed upon return to long-term varying climatic conditions. The Early–Middle Eocene long-term climatic trend was instead coeval to true evolutionary trends with the appearance of the very successful *Noelaerhabdaceae* clade whose offsprings include the most important bloom-forming coccolithophorids in the modern ocean. The Early–Middle Eocene can thus be considered the time in which nannoplankton communities set course toward modern structure triggering a reconfiguration of the global ocean life chain.

1. Introduction

We present the quantitative nannofossil biostratigraphy and magnetostratigraphy of a ~68-m-thick marine limestone section from Possagno in northern Italy. This section refines the biomagnetostratigraphic record

* Corresponding author. Fax: +39 049 8272070.
  E-mail address: claudia.agnini@unipd.it (C. Agnini).

available for the Late Paleocene–Middle Eocene (e.g., [1]), which is one of the most unusual time intervals in the Cenozoic, when Earth experienced long-term greenhouse conditions lacking polar ice, punctuated by transient temperature excursions such as the Paleocene–Eocene Thermal Maximum (PETM) [2] and the Elmo horizon [3].

Previous studies showed the occurrence in the Possagno area of limestones with planktic foraminifera and calcareous nannofossils of Paleocene–Eocene age [4–6]. The Possagno section of this study is located in the Carcoselle quarry, 1.5 km to the west of the town of Possagno (Fig. 1). The section was well exposed and continuous along an active quarry front at the time of

sampling, but, because of later extraction activity, the section is at present largely covered and inaccessible. The basal 21 m of the section consists of finely bedded red limestones of the Scaglia Rossa (Red Scaglia) Formation that straddle a 30-cm-thick interval of dark-red marly clays–informally termed Marly Clay Level–characterized by high carbonate dissolution and/or clay content (Fig. 2). The base of the Marly Clay Level coincides with a $\delta^{13}C$ negative excursion [6] that is virtually coincident with the Paleocene–Eocene boundary according to planktic foraminifera [6] and calcareous nannofossils (this study) (Fig. 2). The Scaglia Rossa is overlain by 47 m of finely bedded marly limestone beds of red, white and grey color of the Scaglia Varie-
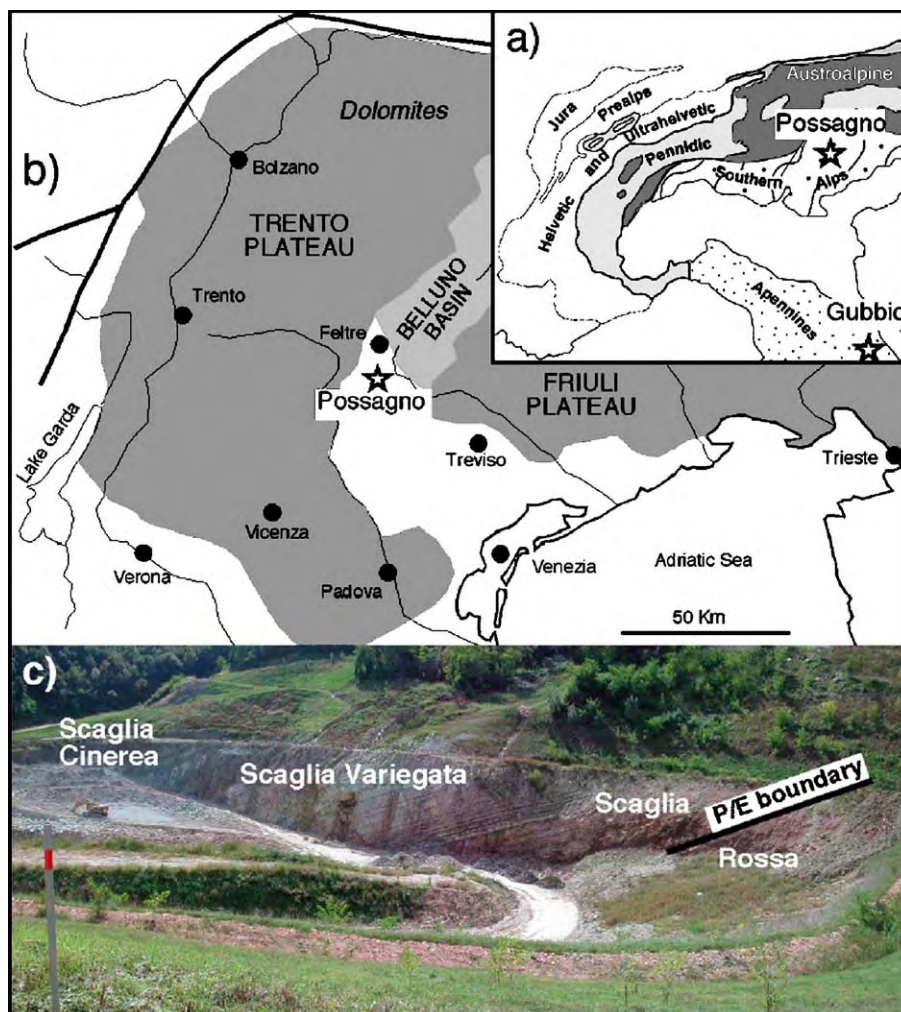

Fig. 1. (a) The Possagno section is located in the eastern Southern Alps, whereas the coeval Contessa and Bottaccione sections from the literature crop out in the Umbria–Marche Basin near Gubbio; (b) the Possagno section belongs to a Mesozoic–Cenozoic mainly pelagic sequence typical of the Belluno Basin, which is delimited to the west by the Trento Plateau and to the east by the Friuli Plateau; (c) the Possagno section crops out in the Carcoselle quarry, 1.5 km west of the town of Possagno at 45°50′2″N, 11°31′1″E.
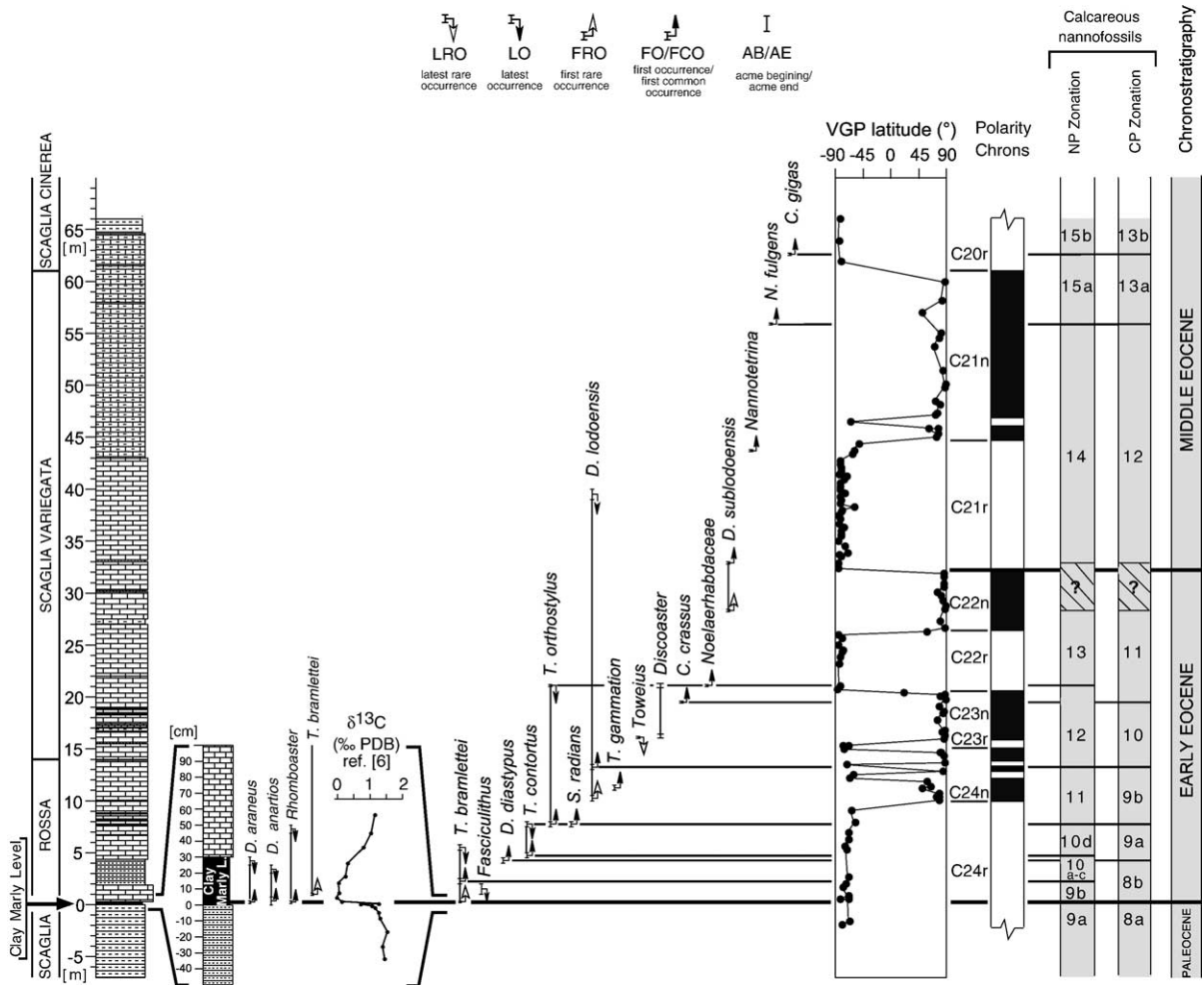
Fig. 2. The Late Paleocene–Middle Eocene Possagno section with indication, from left to right, of lithologic units, $\delta^{13}C$ data from [6] across the Clay Marly Level, calcareous nannofossil biostratigraphic events, latitude of the sample VGP relative to the north pole of the mean paleomagnetic axis with magnetic polarity zones shown by filled (open) bars for normal (reverse) polarity placed next to standard nannofossil zonations and chronostratigraphic interpretation. See text for discussion.

gata (Multi-hued Scaglia) Formation, followed by 5 m of clay-rich limestone beds of the Scaglia Cinerea (Grey Scaglia) Formation.

2. Calcareous Nannofossil quantitative biostratigraphy

2.1. Materials and methods

A mixed approach was adopted involving traditional data (e.g., species first occurrence, last occurrence) and species quantitative distribution patterns (e.g., cross-over, acme), which has proved to be a reliable tool for improving biostratigraphic resolution. A total of 330 samples were collected, 200 of which were prepared using standard methods and analyzed. Samples

were taken every 5–10 cm from −2.5 to 1 m, every 20 cm up to the 25 m level and on average every 1–2 m throughout the rest of the section with local refinements (every 20 cm) close to relevant biostratigraphic events. Smear slides were studied in light microscopy at 1250× magnification. Microphotographs of significant calcareous nannofossil taxa are shown in Fig. 1 in the Appendix.

Biostratigraphic events are defined as species first rare occurrence (FRO), first occurrence (FO), first common occurrence (FCO), last rare occurrence (LRO), last occurrence (LO), acme beginning (AB), acme end (AE) and cross-over (CO). A standard taxonomy after Aubry [7–11] and Perch-Nielsen [12] was adopted, whereas the zonation schemes were those of Martini [13] (NP) and Okada and Bukry [14] (CP).

The abundance patterns of *Coccolithus crassus*, *Toweius*? *gammation* and the cross-over between *Toweius* and *Dictyococcites/Reticulofenestra* were determined by counting 300 specimens of the total sample assemblage. The abundance patterns of species of *Discoaster* and *Sphenolithus* were determined by counting a prefixed number of taxonomically related forms [15], i.e., 50 discoasterids and 100 sphenoliths, respectively. The abundance patterns of *Fasciculithus* and *Zygrhablithus* were determined by counting index species in a prefixed area (1 mm^2) [16]. The abundances of the rare taxa *Rhomboaster*, *Tribrachiathus bramlettei*, *Tribrachiathus contortus*, *Tribrachiathus orthostylus*, *Nannotetrina*, *Nannotetrina fulgens* and *Chiasmolithus gigas* were determined by counting index species in

three smear slide tracks normalized to a prefixed area (1 mm^2).

2.2. Results

The nannofossil assemblage is generally rich and well diversified and the preservation varies from poor to moderate. Reworked forms are rare. The following biostratigraphic events (Fig. 2 and Table 1 in the Appendix) and species quantitative distribution patterns (Fig. 3) are described from section base to top.

(i) The FO and LO of *Discoaster araneus* occur at 1.8 cm and 28 cm, respectively, the FO and LO of *Discoaster anartios* at 2.5 cm and 22.5 cm,
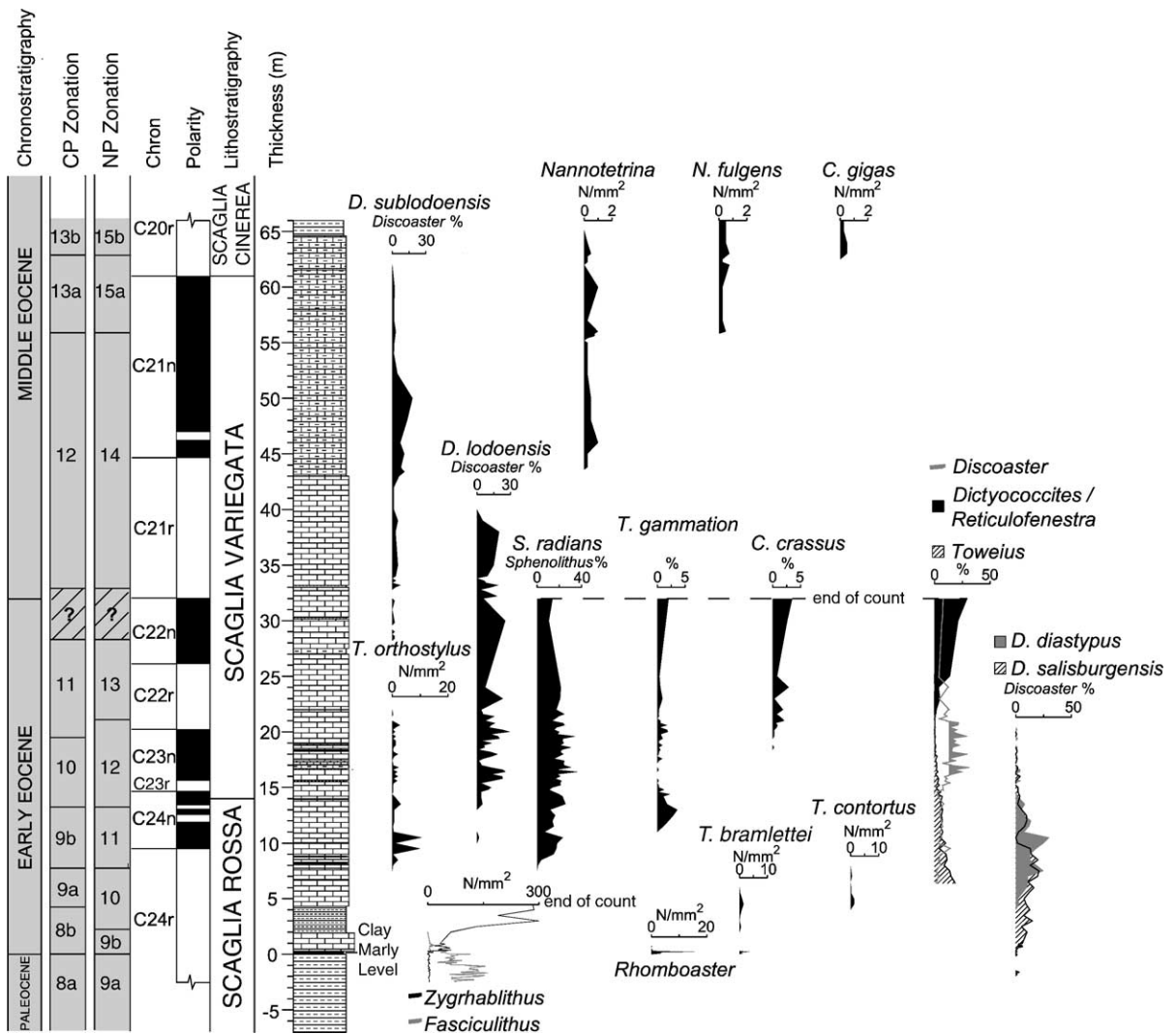

Fig. 3. Abundance patterns of selected nannofossil species and genera from the Possagno section are plotted against chronostratigraphy, calcareous nannofossils biostratigraphy, magnetostratigraphy and lithostratigraphy. See text for discussion.

respectively, and the FO and LO of *Rhomboaster* at 1.8 cm and 47.5 cm, respectively. These species belong to the Calcareous Nannofossil Excursion Taxa (CNET)–also known as the *Rhomboaster–Discoaster* (RD) association–typical of the base of the Eocene and restricted to the PETM [17–21]. We used the FO of *Rhomboaster* to subdivide Zone CP8 into Subzones CP8a and CP8b [22], and the FO of CNET to subdivide Zone NP9 into Subzones NP9a and NP9b [23].

(ii) The LO of *Fasciculithus* occurs at 1.5 m. In the basal Eocene stratotype at Dababiya (Egypt), the Paleocene–Eocene boundary slightly predates the LO of *Fasciculithus* [24]. Quantitatively, fasciculiths show a sharp drop of abundance at 0.3 m that coincides with the CO between *Zygrhablithus* and *Fasciculithus*, as observed also elsewhere [25–27].

(iii) *T. bramlettei* FRO, FO and LO occur at 7.5 cm, 2.25 m and 5.75 m, respectively; the interval between its FRO and FO contains no *T. bramlettei*. *T. bramlettei* is believed to possess either a rhombohedral structure [28–30] or a triradiate symmetry [31–33]. Bearing in mind the debatable taxonomy, we used the FO of *T. bramlettei* to mark the base of Zone NP10 [18,34].

(iv) The FCO of *Discoaster salisbugensis* occurs at 0.4 m and the FO of *Discoaster diastypus* at 4.25 m. We assigned to *D. diastypus* specimens larger than 15 μm in size and with number of rays ranging from 14 to 20, and to *D. salisburgensis* specimens ranging in size from 8 to 15 μm and with number of rays ranging from 13 to 26. We used the FO of *D. diastypus* to identify the base of Zone CP9 [14]. Quantitatively, both species show a sharp increase of abundance at their FOs and a gradual decrease of abundance in levels below their LOs.

(v) The FO of *T. contortus* occurs at 4.75 m and the LO of *T. bramlettei* at 5.75 m, with transitional forms observed in the overlap interval. We used the FO of *T. contortus* to mark the base of Subzone NP10d [33]. The FO of *T. contortus*, detected immediately above the FO of *D. diastypus* (see iv) as observed also by Raffi et al. [21], represents an auxiliary marker of the base of Zone CP9. No specimens of *Tribrachiathus digitalis* [33] were confidently identified.

(vi) The LO of *T. contortus*, the CO between *T. contortus* and *T. orthostylus*–described by Perch-Nielsen [12] and Backman [18]–as well as the

FO of *Sphenolithus radians* occur at 7.75 m. We used the LO of *T. contortus* to identify the base of Zone NP11. *T. contortus* shows low abundance values especially slightly below its LO.

(vii) The FOs of *T. orthostylus* and *S. radians* occur at 7.75 m at the base of Zone NP11 (see vi). We regard the FO of *S. radians* particularly useful to approximate the base of Zone NP11 in case *Tribrachiathus* is missing. *T. orthostylus* and *S. radians* show a sharp increase of abundance at their FOs.

(viii) The FO of *T.? gammation* occurs at 11.25 m within Zone NP11, slightly below the FO of *Discoaster lodoensis* (see ix). *T.? gammation* shows a sharp rise of abundance at its FO.

(ix) The FRO and FO of *D. lodoensis* occur at 10.25 m and 13.25 m, respectively; the intervening interval contains no *D. lodoensis*. We used the FO of *D. lodoensis* to mark the base of Zone NP12 (correlative to Zone CP10). A sharp and continuous increase of abundance characterizes *D. lodoensis* FO.

(x) A relative high-abundance interval of discoasterids, termed the *Discoaster* Acme, with abundance values ranging 15–30% of the total assemblage (average of ~20%) begins at 16.10 m and ends at 20.90 m. In this interval, specimens of *Toweius* are rare to absent (<0–2%; *Toweius* LRO). The FCO of *Noelaerhabdaceae* [35] occurs at 20.90 m around the NP12–NP13 zonal boundary with specimens of the *Dictyococcites/Reticulofenestra* group exhibiting abundances >1.5–2% of the total assemblage. At this level (20.90 m), *Discoaster* shows a sharp decrease of abundance from 10–12% to 3.7% of the total assemblage.

(xi) The FO of *C. crassus* occurs at 19.50 m and marks the base of Zone CP11 [14]. Quantitatively, its initial discontinuous presence is followed by a conspicuous and continuous entry occurring before the LO of *T. orthostylus* at 20.90 m.

(xii) The FRO and FO of *Discoaster sublodoensis* occur at 28.30 m and 32.90 m, respectively. The FO of *D. sublodoensis* is used to define the base of Zone NP14 (correlative to Zone CP12), which predates the base of the Middle Eocene (Lutetian) as defined by foraminifera (FO of *H. nuttalli*, [1]). *D. sublodoensis* is strictly related to *D. lodoensis* and transitional forms were observed in the species overlap interval. This, coupled with re-crystallization and poor preservation of tests, frequently hampered their distinction. In addition, *D. sublodoensis* is exceedingly rare and

exhibits a discontinuous abundance pattern, especially in the lower part of its range.

(xiii) The LO of *D. lodoensis* occurs at 39.50 m. A sharp decline of abundance was detected in levels below its LO.

(xiv) The FO of *Nannotetrina* occurs at 43.70 m and the FO of rare specimens of *N. fulgens* at 55.70 m. We used this latter event to mark the base of Zone NP15 (correlative to Zone CP13).

(xv) The FO *C. gigas* is located at 62.60 m and was used to mark the base of Zone CP13b. *C. gigas* shows an overall scarce abundance pattern.

In summary, the Possagno section spans a Late Paleocene–Middle Eocene time interval encompassing Zones NP9–NP15 (equivalent to Zones CP8–CP13b) (Figs. 2 and 3; Table 1 in the Appendix). Following the directives of the recently ratified Eocene stratotype at Dababiya (Egypt) [17], the Paleocene–Eocene boundary was placed at the base of the $\delta^{13}C$ negative excursion located at the base of the Marly Clay Level [6], which virtually coincides (within 2 cm) with the base of Zone NP9b established by using the FOs of *D. araneus* and *Rhomboaster* [19]. The base of the Middle Eocene (Lutetian) could be only roughly approximated by the FO of *D. sublodoensis* at the base of Zone NP14 [1,36]. We show below that magnetostratigraphic correlation to the Berggren et al. [1] time scale constrains the base of the Middle Eocene to the base of Chron C21r at the 32.03 m level.

Quantitatively, the lower part of the section essentially consists of *Coccolithus* and *Toweius* in association with *Ericsonia*, *Prinsius*, *Fasciculithus*, *Sphenolithus*, *Octolithus* and *Zygrhablithus*. The CO between fasciculiths and *Zygrhablithus* occurs at 0.30 m, whereas the CO between *Prinsiales* and *Noelaerhabdaceae* occurs in the 16.10–20.90 m interval. The *Noelaerhabdaceae* family underwent a relevant evolutionary step consisting of a simplification of the coccolitophores structure with respect to *Prinsiales* building [35]. The more evolved *Dictyococcites*/*Reticulofenestra* group replaced *Toweius* and, in the cross-over interval, *Discoaster* flourished, reaching abundance values up to ~30% of the total assemblage. We will return to this evolutionary path in the concluding remarks of this paper. In the upper part of the section, *Reticulofenestra* and *Dictyococcites* dominate over *Coccolithus*, *Ericsonia*, *Sphenolithus* and *Zygrhablithus*. *Triquetrorhabdolus* and *Nannotetrina* show high relative abundance and rare occurrence values, respectively. *Chiasmolithus* displays an up-section increase of abundance and size.

3. Paleomagnetism

Paleomagnetic samples were drilled and oriented in the field at an average sampling interval of ~0.5 m giving a total of 122 standard ~11 cc specimens for analyses, conducted at the paleomagnetic laboratory of Lamont-Doherty Earth Observatory.

The intensity of the natural remanent magnetization (NRM), measured on a 2G DC-SQUID cryogenic magnetometer, ranges between 0.05 and 10 mA/m with lowest values in the central part of the sampled section. A representative suite of samples was subjected to rock magnetic analysis using isothermal remanent magnetization (IRM) backfield acquisition curves (up to 2.5 T). Samples showed three types of behaviors (Fig. 4a): (i) IRM initially increased steeply resulting in a relatively low coercivity of remanence (Bcr) of ~0.1 T, then continued to climb gently only approaching saturation by ~1.5 T field; (ii) IRM climbed initially less steeply resulting in moderate Bcr values of ~0.25 T, then continued to climb gently approaching saturation by ~1.5 T field; (iii) IRM climbed initially steeply but reached an apparent plateau by ~0.15 T and, from ~0.4 T onward, IRM continued to increase resulting in high Bcr values of ~0.9 T and no tendency to saturate even in a field of 2.5 T. This suggests a composite magnetic mineralogy with contrasting coercivities whereby case (i) samples may be dominated by a magnetite–hematite mixture, case (ii) samples by fine-grained hematite and case (iii) samples by very high coercivity minerals such as goethite coexisting with minor amounts of magnetite.

All samples were thermally demagnetized in 50 °C steps from room temperature to 680 °C; the component structure of the NRM was monitored after each demagnetization step by means of vector end-point demagnetization diagrams [37], and steps of 25–10 °C were adopted close to critical unblocking temperatures. Magnetic components were calculated by standard least-square analysis [38] on linear portions of the demagnetization paths and plotted on equal-area projections.

A large decrease of NRM values was observed between room temperature and ~100 °C and was associated with scattered component directions that persisted up to maximum demagnetization treatments of ~250–350 °C; these components are interpreted as associated with surface weathering (formation of goethite) and/or imparted during sampling. Removal of these spurious magnetizations revealed the presence of a characteristic component linearly trending to the origin of the demagnetization axes. This characteristic component was isolated in 120 (98%) of the specimens by linear interpolation of an average of 13 demagneti-
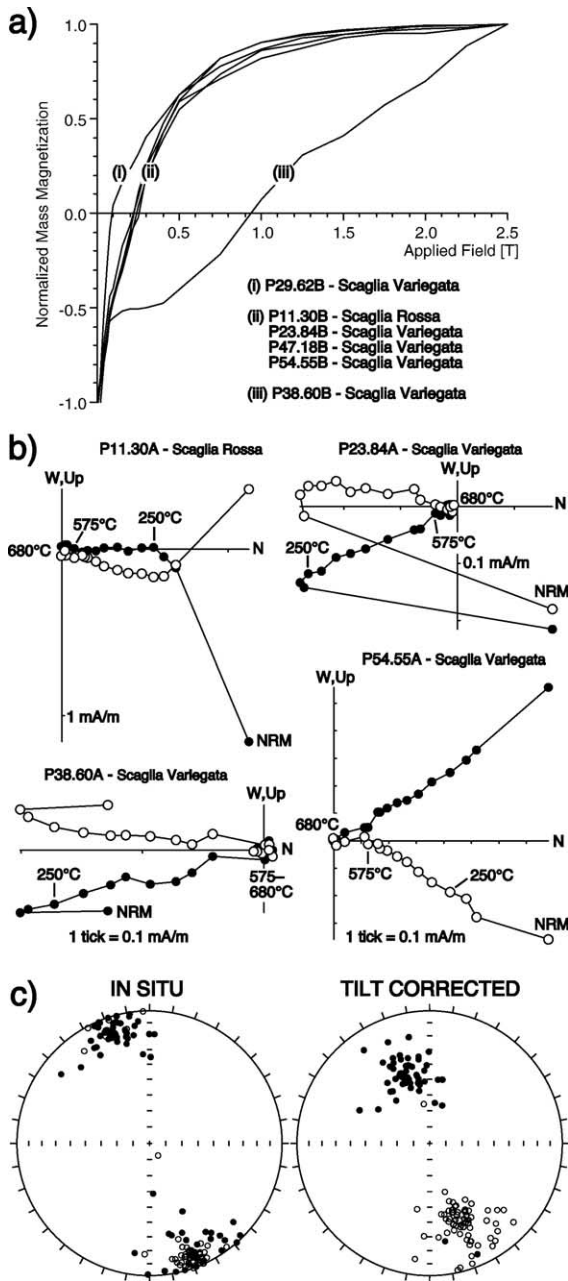
Fig. 4. (a) Isothermal remanent magnetization (IRM) backfield acquisition curves of representative samples from Possagno. (b) Vector end-point demagnetization diagrams of representative samples from Possagno. Closed symbols are projections onto the horizontal plane and open symbols onto the vertical plane in geographic (in situ) coordinates. Demagnetization temperatures are expressed in °C. (c) Equal-area projections before (in situ) and after bedding tilt correction of the characteristic component directions (Table 1). Closed symbols are projections onto the lower hemisphere and open symbols onto the upper hemisphere.

zation steps from ~250–350 °C to 575 °C or 650–680 °C (average MAD value of $7° ± 3°$). Maximum unblocking temperatures of 575 °C or 650–680 °C and the IRM acquisition data used in conjunction with sediment color point to hematite as the main magnetic carrier in reddish Scaglia Rossa samples and a variable mixture of magnetite and hematite in greenish-reddish Scaglia Variegata samples, as commonly observed in Paleocene–Eocene Scaglia limestones from the Umbrian Apennines [39]. These characteristic magnetizations are oriented northwest and shallow down or southeast and shallow up in geographic (in situ) coordinates and, after correction for homoclinal bedding tilt, they acquire steeper inclinations (Fig. 4c). These populations depart from antipodality by ~11°, which we attribute to residual contamination from lower temperature components, and the reversal test [40] is statistically negative. The effect of the contaminating bias on the mean direction could be minimized by inverting all directions to common polarity, which resulted in a tilt corrected mean direction of Dec. = 339°, Inc. = 37.5° ($k = 19$, $\alpha_{95} = 3°$; Table 1).

To constrain the age of the characteristic magnetization and assign polarity to the northwest and down or southeast and up characteristic directions, we compared the mean paleopole from Possagno, obtained by averaging the virtual geomagnetic poles (VGPs) corresponding to the characteristic component directions

Table 1
Characteristic component directions and paleomagnetic pole from Possagno

N	MAD	Geographic (in situ) coordinates				Bedding (tilt-corrected) coordinates			
		k	α_{95}	GDEC	GINC	k	α_{95}	BDEC	BINC
Normal polarity directions									
52	6 ± 3	32	3.5	342.0	10.7	32	3.5	341.2	43.7
Reverse polarity directions									
68	7 ± 4	17	4.4	158.6	0.1	17	4.4	157.5	−32.7
Reverse and normal polarity directions									
120	7 ± 3	19	3.0	340.1	4.7	19	3.0	339.0	37.5
Paleomagnetic pole									
N	K	A_{95}	LONG	LAT					
120	25.2	2.6	233.1	60.1					

N = number of samples; MAD = mean angular deviation of the mean paleomagnetic direction expressed in degrees; k and K = Fisher precision parameter of the mean paleomagnetic direction and pole, respectively; α_{95} and A_{95} = Fisher angle of half cone of 95% confidence about the mean paleomagnetic direction and pole, respectively; GDED and GINC = declination and inclination in geographic (in situ) coordinates of the mean paleomagnetic direction; BDED and BINC = declination and inclination in bedding (tilt-corrected) coordinates of the mean paleomagnetic direction; LONG and LAT = longitude and latitude of the mean paleomagnetic pole.

(Table 1), to a Late Cretaceous–Pliocene apparent polar wander (APW) path for Africa, constructed by integrating paleopoles from Tauxe et al. [41] and Schneider and Kent [42] (Fig. 5a). The Possagno paleopole falls close to the Africa APW path but is rotated 13–20° counterclockwise with respect to Africa Paleocene–Eocene reference paleopoles. This suggests substantial paleogeographic affinity of the Southern Alps with Africa and tectonic rotation of thrust sheets that occurred during Alpine deformation in the Cenozoic [43]. Thrust sheet rotations are common in the deformed margin of Adria in the Southern Alps and the Apennines [44]. However, relatively less deformed regions of Adria such as the Adriatic foreland or portions of the Southalpine chain (e.g., the Dolomites) maintained substantial tectonic coherence (within paleomagnetic resolution) with Africa during Alpine deformation [45–47]. As evidence of this, a Late Cretaceous mean paleopole for Adria (Ku2), obtained by averaging paleopoles mainly from the Adriatic foreland (Iblei, Gargano, Istria) and the Southern Alps listed in Channell [48], is virtually undistinguishable from the coeval Africa reference paleopole (Ku1; [41]). We therefore assume that before Alpine deformation the Southern Alps were tectonically coherent with Adria, which was a promontory of Africa. We placed Adria in a paleogeographic reconstruction by using the Paleocene Africa paleopole of [42] and restoring other Gondwanan and Laurasian elements relative to Africa using published Euler poles of rotation for magnetic Anomaly 25 (Chron C25n) (Fig. 5b). In the Paleocene, Adria was located at tropical paleolatitudes in the northern hemisphere. Consequently, the northwest and down or southeast and up characteristic directions are regarded as acquired close to the time of sediment deposition during normal or reverse geomagnetic field polarity, respectively.

4. Magnetostratigraphy and age model

The latitude of the sample characteristic magnetization VGP relative to the mean paleomagnetic (north) pole axis was used for interpreting polarity stratigraphy [49,50]. VGP relative latitudes approaching +90°N or −90°N are interpreted as recording normal or reverse polarity, respectively. An overall sequence of 13 magnetozones was integrated with the biostratigraphic information outlined above (Fig. 2).

We compared data from Possagno to data from classic coeval sections of similar Scaglia facies outcropping in the Northern Apennines near Gubbio. Similarities in the nannofossil zonation and an excellent overall magnetostratigraphic agreement were observed between Possagno and the Bottaccione, Contessa Highway and Contessa Road sections [50–52] (Fig. 6). All these magnetostratigraphic sections can be correlated to the stacked profiles of magnetic anomalies 24–20 from the South Atlantic [53].

We constructed an age–depth plot and derived sediment accumulation rates and the age of the biostratigraphic events at Possagno by magnetostratigraphic correlation to the geomagnetic polarity time scale of Cande and Kent [54] (CK95) assuming constant sediment accumulation rates between magnetochron boundaries (Fig. 7, Table 1 in the Appendix). The base of the sampled succession does not extend to the C25n–C24r boundary; therefore, we had to adopt as the lowermost
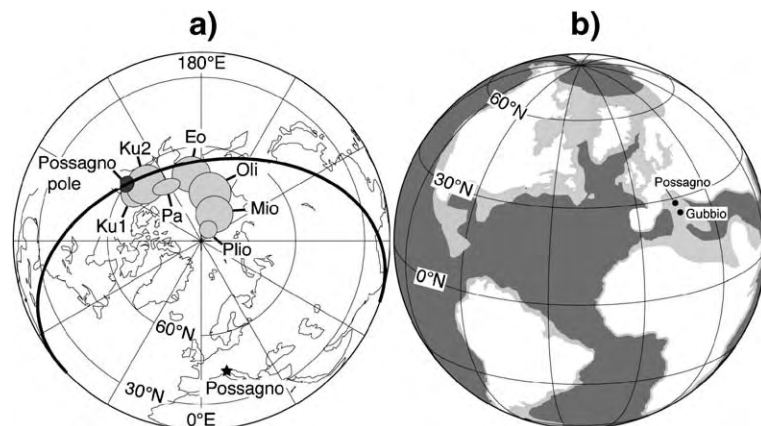

Fig. 5. (a) The mean paleopole from Possagno (Table 1) is compared to a reference Late Cretaceous–Pliocene African apparent polar wander path constructed by integrating data from [41] (K1=Late Cretaceous, Eo=Eocene, Oli=Oligocene, Mio=Miocene and Plio=Pliocene) and [42] (Pa=Paleocene). A mean Late Cretaceous paleopole for tectonically unrotated Adria derived from [48] (K2; lat.=64.2°, long.=234.5°E, k=118, α_{95}=4.5, N=10) is plotted for comparison to the African K1 paleopole. (b) Adria is placed in a global paleogeographic reconstruction by using the Paleocene African paleopole and published Euler poles of rotation [71–74] centered at marine magnetic anomaly 25 time.
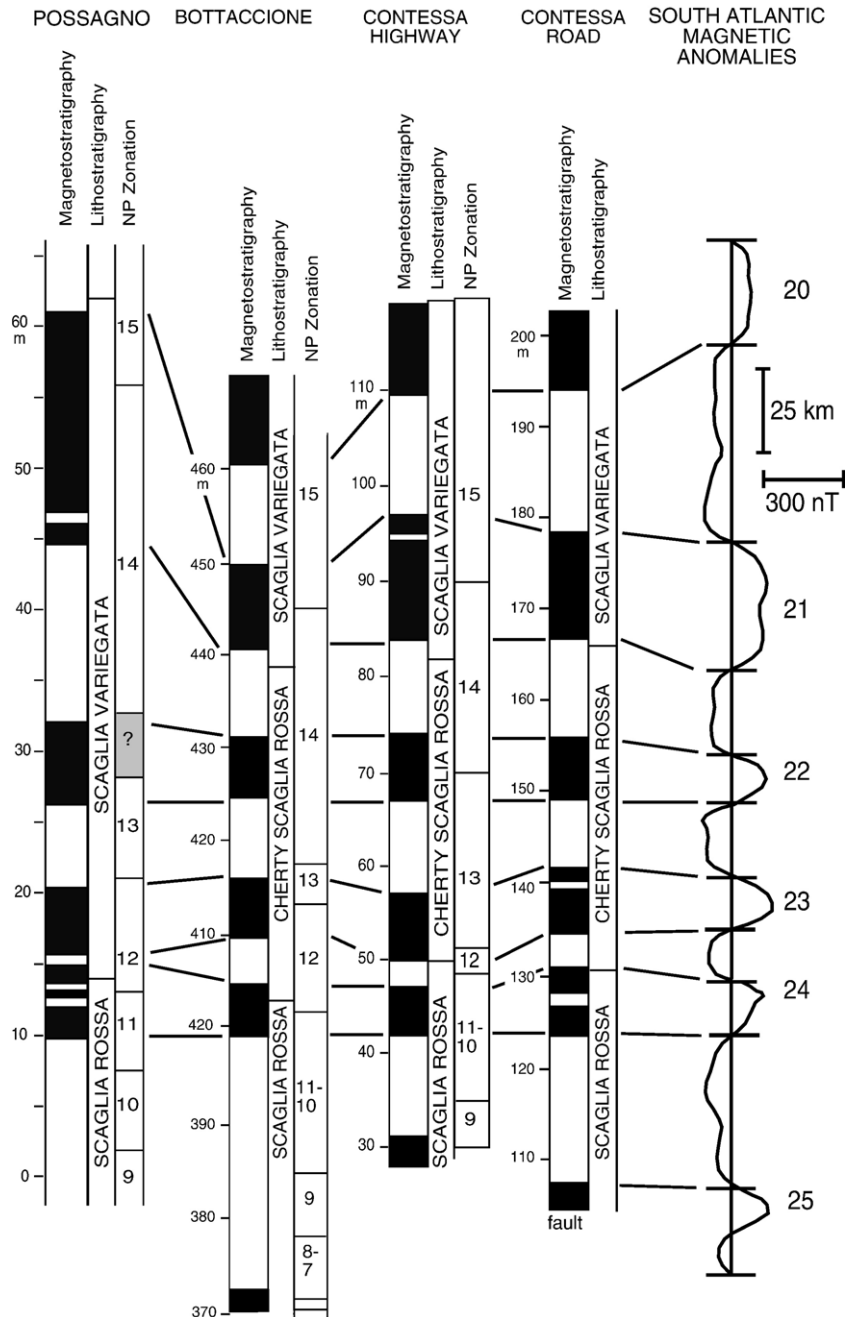
Fig. 6. Correlation of Possagno magnetobiostratigraphy to the classic Bottaccione, Contessa Highway and Contessa Road [50–52] sections near Gubbio in the Northern Apennines (Italy), as well as to a composite stacked profile of South Atlantic marine magnetic anomalies [54].

pair of chronologic control points the Paleocene–Eocene boundary placed at 55.16 Ma [23] and the base of Chron C24n. The age model derived using CK95 implies sediment accumulation rates that on average are controlled by lithology (Fig. 7). Rates of ~5–6 m/m.y. characterize the Scaglia Rossa interval from the Paleocene–Eocene boundary up to the base of Chron

C24n. Localized perturbations of sediment accumulation rates are observed across the Scaglia Rossa–Scaglia Variegata transition with a notable decrease to ~1 m/m.y. during Chron C23r in the lowermost Scaglia Variegata where a ~20-cm-thick marly interval of possible condensation is present at 15.5 m. The overlying Scaglia Variegata marly limestones were deposited at
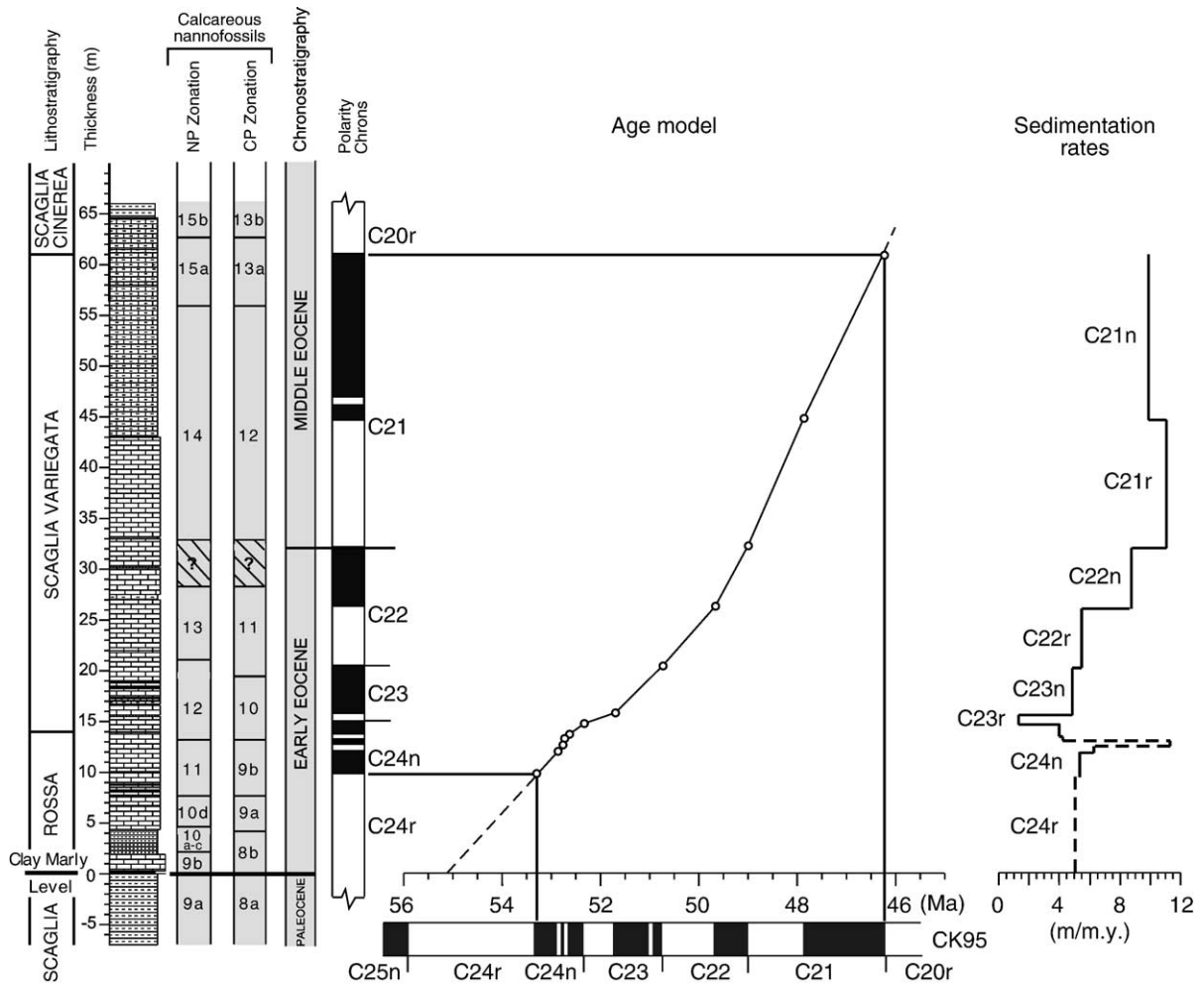
Fig. 7. Age–depth model and derived sediment accumulation rates for the Possagno section obtained by magnetostratigraphic correlation to the geomagnetic polarity time scale of Cande and Kent [54] (CK95).

rates smoothly increasing from ~5 to ~10 m/m.y. and this trend corresponds to an up-section increase of clay content.

5. Age of biostratigraphic events

The calculated sediment accumulation rates were used to calibrate key calcareous nannofossil events at Possagno for comparison with parallel events in the Berggren et al. [1] time scale (BKSA95) (Fig. 8, Table 1 in the Appendix). We adopted a slightly modified version of the BKSA95 in which Zone NP9 is subdivided into Subzones NP9a and NP9b [23] and Zone NP10 into Subzones NP10a–NP10d [33]. The Paleocene–Eocene boundary is approximated by the base of Zone NP9b at 55.16 Ma [19,1] modified after [23], whereas the base of the Middle Eocene (Lutetian) coincides with the base of Chron C21r at 49 Ma [1].

Inspection of Fig. 8 reveals that the Possagno section and the BKSA95 time scale bear an overall correlative nannofossil sequence straddling Zones NP9–NP15b and CP8–CP13b. Starting from the section base and referring for simplicity only to the NP zonation, the largest offsets between Possagno data and the BKSA95 time scale were detected for Zones NP9–NP11 within C24r. However, these uncertainties could be due to the fact that the Possagno section lacks the base of C24r (and cycle stratigraphy) for better age constraints. Good to reasonable agreement was observed for the base of Zone NP12 (*D. lodoensis* FO) within C24n, the base of Zone NP13 (*T. orthostylus* LO) close to the base of C22r, the base of Subzone NP15a (*N. fulgens* FO) in the mid-portion of C21n and the base of Subzone NP15b (*C. gigas* FO) close to the base of C20r. The moderate offset observed for the base of Zone NP14 in the C22n interval is due to difficulties in locating *D. sublodoensis* FO as described
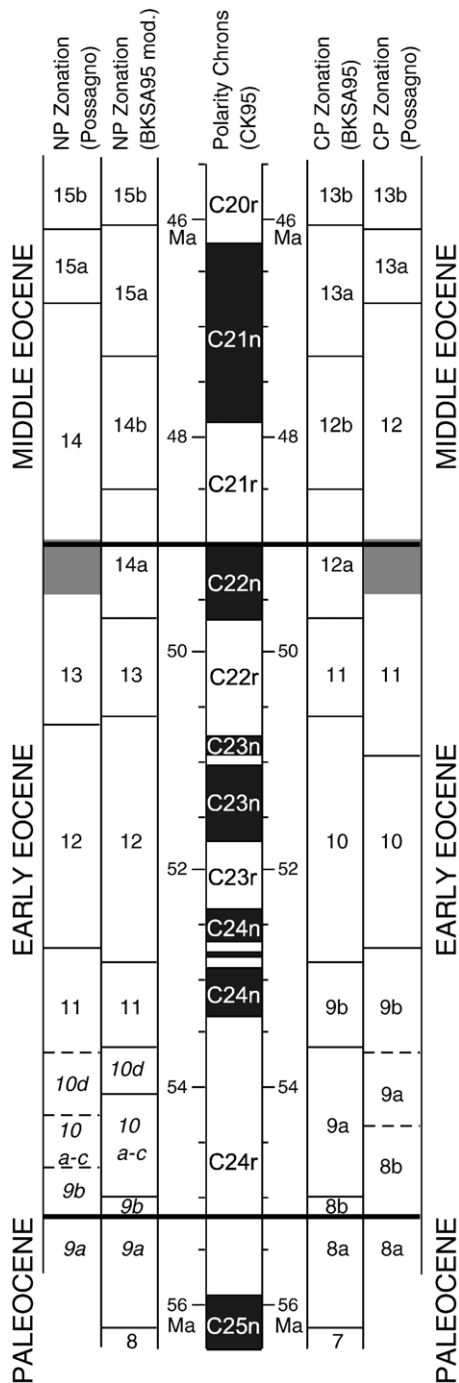
Fig. 8. Comparison of Possagno nannofossil zonations to parallel zonations used in the timescale of Berggren et al. [1] (BKSA95) via common correlation to the geomagnetic polarity time scale of Cande and Kent [54] (CK95). In the NP Zonation column, "BKSA95 mod." refers to a slightly modified version of the BKSA95 in which Zone NP9 is subdivided into Subzones NP9a and NP9b [27] and Zone NP10 into Subzones NP10a–NP10d [33] (in italics on figure). The Paleocene–Eocene boundary is approximated by the base of Zone NP9b at 55.16 Ma [19,1] modified after [23], whereas the base of the Middle Eocene (Lutetian) by the base of Chron C21r [1].

in paragraph (xii) of the biostratigraphy chapter. Additional correlative biostratigraphic events–not listed in Fig. 8 because they define as yet no zonal boundaries–are the *D. lodoensis* LO within Zone NP14 in the upper half of C21r and *Nannotetrina* FO within Zone NP14 close to the C21r–C21n boundary (Table 1 in the Appendix). Finally, we have calculated relative to magnetochrons the positions of some new or as yet poorly tested events, i.e. *T.? gammation* FO in the lower half of C24n, *Toweius* LRO and *Discoaster* AB in the lower half of C23n, *Discoaster* AE and *Dictyococcites/Reticulofenestra* FCO in the lower half of C22r (Table 1 in the Appendix); notably, this last mentioned event was detected at Possagno in levels several million years older than previous estimates (Chron C18r–Zone NP16) [55]. In this respect, we tend to exclude the possibility of down-section contamination because of the continuous presence and relatively high abundance of *Dictyococcites* from its first occurrence up to the section top.

6. The calcareous nannofossil response to climate change

Data from Possagno were correlated to the oxygen isotope record of Zachos et al. [2], which was calibrated with the BKSA95 time scale [1], to investigate the temporal relationships between nannofossil turnovers and climate variability in the Late Paleocene–Middle Eocene. The benthic foraminifera record [2] shows a long-term $\delta^{18}O$ decrease of $\sim 1\permil$ interpreted as a warming trend that started in the Paleocene and culminated in the Early Eocene Climatic Optimum (EECO), and a Middle–Late Eocene $\delta^{18}O$ increase interpreted as a cooling trend that climaxed at the Eocene–Oligocene boundary (Fig. 9). Superposed on this long-term variability are transient events such as the PETM at the Paleocene–Eocene boundary, visible in the $\delta^{18}O$ record as a $\sim 1.2\permil$ negative excursion [2] paralleled by a $\delta^{13}C$ negative excursion of $\sim 3\permil$ (CIE) [56] of ~ 220 kyrs duration [57] presumably due to the massive and abrupt input of CO_2 [3,58–61], triggered by a mechanism as yet elusive, which increased pCO_2 and acidity values in the oceans as well as global temperatures by several °C [2,62,63].

Biotic responses coeval to both the short-lived PETM and the Eocene long-term climatic trend can be recognized at Possagno. Nannofossils characterizing the CNET association were found in levels broadly restricted to the Clay Marly Level where a negative carbon isotope excursion was found [6] (Fig. 2) that correlates to the carbon (and oxygen) isotope excursion that globally marks the PETM (Fig. 9). The CNET consist of anom-
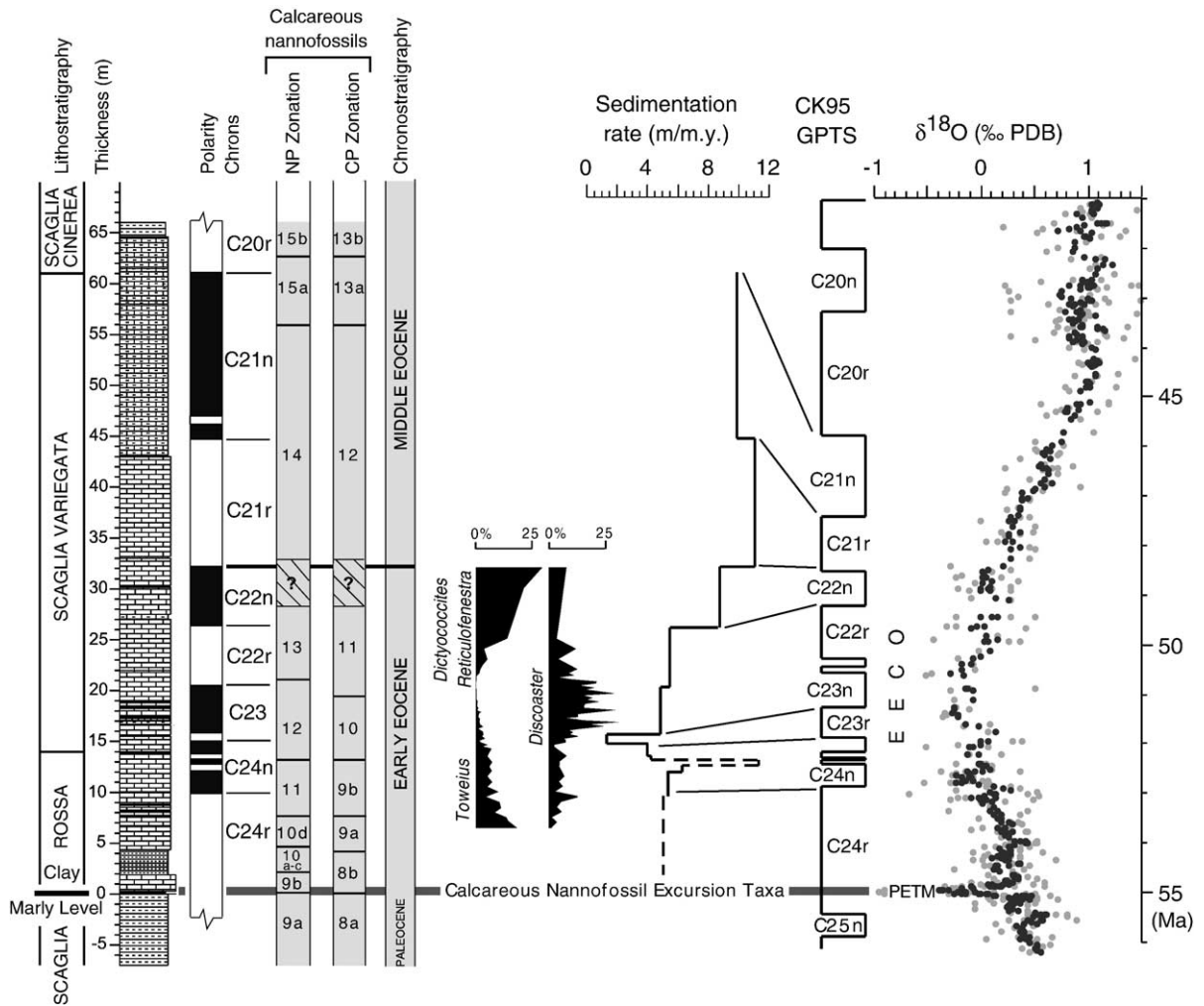
Fig. 9. Possagno biomagnetostratigraphy and key quantitative nannofossil distributions (*Discoaster*, *Dictyococcites*/*Reticulofenestra* and *Toweius*) are compared to the Cande and Kent [54] Geomagnetic Polarity Time Scale (CK95) and the benthic foraminifera oxygen isotope record of [2] (www.es.ucsc.edu/%7Esilab/ZACPUBDATA/2001CompilationData). In the isotope record, black dots represent five-point running averages of the original data (grey dots). See text for discussion.

alous short-lived taxa [19,24] that are probably ecophenotypes [20] developed in response to transient chemical modifications of the world's oceans. Results obtained in laboratory-cultured coccolithophorids show that high levels of pCO_2 can produce a biocalcification crisis and the appearance of malformed coccolitophores tests [64]. These ecophenotypic adaptations were reabsorbed upon return to normal climatic conditions (i.e. long-term varying) because the CNET were restricted to the PETM; only the *Rhomboaster*/*Tribrachiathus* lineage survived the PETM although it never became dominant throughout the Early Eocene. The Clay Marly Level containing the CNET represents a marked increase in carbonate dissolution and/or terrigenous input observed regionally in the Belluno basin of the Southern Alps (L. Giusberti, 2005, pers. comm.), presumably related to high values of

pCO_2 that increased the dissolution of calcite shells of microplankton and/or enhanced weathering.

The following sequence of events characterizes the onset of EECO at Possagno (Fig. 9):

(i) Stratigraphic levels of ~C24r–C24n age, which are correlative to the $\delta^{18}O$ decreasing (warming) trend leading to EECO, are characterized by a progressive decrease in abundance of *Prinsiales* (namely *Toweius*) and low percentages of *Discoaster*.

(ii) Stratigraphic levels of ~C23n age, correlative to EECO $\delta^{18}O$ minima, are characterized by the *Discoaster* Acme and the virtual absence of *Prinsiales* (*Toweius*).

(iii) Stratigraphic levels of ~C22r age, which are broadly correlative to the onset of the $\delta^{18}O$ in-

creasing (cooling) trend, are characterized by the end of the *Discoaster* Acme and the early entry of specimens of the *Reticulofenestra/Dictyococcites* group (*Noelaerhabdaceae*).

(iv) Stratigraphic levels of ~C22n age are characterized by an increasing abundance of *Reticulofenestra/Dictyococcites* and low percentages of *Discoaster*.

In modern oceans, the role of temperature and trophic levels in shaping the nannoplankton communities can be reasonably disentangled. By contrast, their effects on fossil planktic assemblages are difficult to interpret. Bearing in mind this problem and that *Discoaster* is considered a warm-water taxon thriving in oligotrophic conditions [20,65], whereas *Toweius* as well as the *Reticulofenestra/Dictyococcites* group are thought to prefer colder and more eutrophic waters [66], we put forward two possible scenarios that can explain the sequence of nannoplankton events described above as the result of either water temperature or trophic level variations. In the first scenario, the *Discoaster* Acme was controlled by the onset and decline of EECO warm water temperatures, assuming that the Possagno area was located at the periphery of the paleoecological (temperature) tolerance of *Discoaster* such that relatively minor temperature variations could have had drastic effects on the discoasterids distribution. In the second scenario, oligotrophic conditions controlled the *Discoaster* Acme, while the first entry of *Reticulofenestra/Dictyococcites* was possibly favored by a sharp increase in nutrient availability. Although these changes in calcareous nannofossil assemblages are difficult to interpret, the point to stress is that the long-term component of the Early Eocene climate led to a true and irreversible evolutionary trend that brought the *Noelaerhabdaceae* clade (*Reticulofenestra/Dictyococcites* group) to proliferate in the world's oceans.

7. Conclusions

The Late Paleocene–Middle Eocene quantitative calcareous nannofossil biostratigraphy and magnetostratigraphy from Possagno show that the section encompasses nannofossil Zones NP9–NP15 (equivalent to CP8–CP13b) and Chrons C24r–C21n. The Paleocene–Eocene boundary was placed at the base of a δ^{13}C negative excursion [6] that virtually coincides (within 2 cm) with the base of Zone NP9b, whereas the base of the Middle Eocene (Lutetian) was placed at the base of Chron C21r. New or as yet poorly tested biostratigraphic

events (e.g., the FO of *Dictyococcites*) are described with the aim to improve the current biochronology in the C24r–C21n interval.

Correlation of the Possagno data to the oxygen isotope record of Zachos et al. [2] via the BKSA95 time scale allows us to describe the temporal relationships between climate variability and changes of calcareous nannofossil assemblages. Modifications of ocean chemistry associated with the PETM caused provisional adaptations in the coccolithophores communities (i.e., CNET) that were reabsorbed upon return to long-term varying climatic conditions. On the contrary, the long-term component of Early Eocene climate was able to generate true and irreversible evolutionary trends. Our record shows that a profound and remarkable modification of the genetic pool of the nannoplankton communities occurred when the very successful *Noelaerhabdaceae* clade appeared at around the time of EECO. Offsprings of the *Reticulofenestra/Dictyococcites* group include *Emiliania huxleyi* and *Gephyrocapsa*, the most important bloom-forming coccolithophorids in the present-day oceans. EECO and the subsequent onset of a long-term cooling trend in the late Early Eocene can therefore be considered the time at which nannoplankton communities set course toward modern structure in close temporal contiguity with another important turnover among the planktonic foraminifera characterized by the appearance of new lineages (Zone P8; [67]) adapted to cooler waters and mesotrophic conditions [68,69]. The initiation of a long-term (stepwise) reconfiguration of the plankton biomass may have controlled a parallel reconfiguration of the global ocean life chain. For example, recent micropaleontological evidence supports a late Early Eocene or early Middle Eocene age for the Kuldana Formation of Pakistan that yielded primitive cetaceans such as *Pakicetus*, mammals adapted to hunting fish [70].

Acknowledgements

Appendix A. Supplementary data

Supplementary data associated with this article can be found, in the online version, at doi:10.1016/j.epsl.2005.11.005.

References

[1] W.A. Berggren, D.V. Kent, C.C. Swisher III, M.-P. Aubry, A revised Cenozoic geochronology and chronostratigraphy, in: W.A. Berggren, et al., (Eds.), Geochronology, Time Scales and Global Stratigraphic Correlation, Soc. for Sediment. Geol., Tulsa, Okla., Spec. Publ., vol. 54, 1995, pp. 129–212.

[2] J.C. Zachos, M. Pagani, L.C. Sloan, E. Thomas, K. Billups, Trends, rhythms, and aberrations in global climate 65 Ma to present, Science 292 (2001) 686–693.

[3] L.J. Lourens, A. Sluijs, D. Kroon, J.C. Zachos, E. Thomas, U. Röhl, J. Bowles, I. Raffi, Astronomical pacing of Late Palaeocene to Early Eocene global warming events, Nature 435 (2005) 1083–1087.

[4] H.M. Bolli (Ed.), Monografia Micropaleontologica sul Paleocene e l'Eocene di Possagno, Provincia di Treviso, Italia, Schweiz, Paläontol. Abh., vol. 97, 1975, 222 pp.

[5] F. Proto Decima, P.H. Roth, L. Todesco, Nannoplancton calcareo del Paleocene e dell'Eocene della sezione di Possagno, in: H.M. Bolli (Ed.), Monografia Micropaleontologica sul Paleocene e l'Eocene di Possagno, Provincia di Treviso, Italia, Schweiz. Paläontol. Abh., vol. 97, 1975, pp. 35–55.

[6] I. Arenillas, E. Molina, B. Schmitz, Planktic foraminiferal and δ^{13}C isotopic changes across the Paleocene/Eocene boundary at Possagno (Italy), Int. J. Earth Sci. 88 (2) (1999) 352–364.

[7] M.-P. Aubry, Handbook of Cenozoic Calcareous Nannoplankton, Book 1, Ortholithae (Discoaster), Micropaleontology Press, American Museum of Natural History, New York, NY, 1984, 263 pp.

[8] M.-P. Aubry, Handbook of Cenozoic Calcareous Nannoplankton, Book 2, Ortholithae (Holococcoliths, Ceratoliths, Ortholiths and Other), Micropaleontology Press, American Museum of Natural History, New York, NY, 1988, 279 pp.

[9] M.-P. Aubry, Handbook of Cenozoic Calcareous Nannoplankton, Book 3, Ortholithae (Pentaliths and Other), Heliolithae (Fasciculiths, Sphenoliths and Others), Micropaleontology Press, American Museum of Natural History, New York, NY, 1989, 279 pp.

[10] M.-P. Aubry, Handbook of Cenozoic Calcareous Nannoplankton, Book 4, Heliolithae (Helicoliths, Cribriliths, Lopadoliths and Other), Micropaleontology Press American Museum of Natural History, New York, NY, 1990, 381 pp.

[11] M.-P. Aubry, Handbook of Cenozoic Calcareous Nannoplankton, Book 5, Heliolithae (Zygoliths and Rhabdoliths), Micropaleontology Press, American Museum of Natural History, New York, NY, 1999, 368 pp.

[12] K. Perch-Nielsen, Cenozoic calcareous nannofossils, in: H.M. Bolli, et al., (Eds.), Plankton Stratigraphy, Cambridge University Press, New York, NY, 1985, pp. 427–554.

[13] E. Martini, Standard tertiary and quaternary calcareous nannoplankton zonation, in: A. Farinacci (Ed.), Proceeding of the 2nd International Conference Planktonic Microfossil, vol. 2, Ed. Tecnoscienza, Roma, 1971, pp. 739–785.

[14] H. Okada, D. Bukry, Supplementary modification and introduction of code numbers to the low-latitude coccolith biostratigraphic zonation (Bukry, 1973, 1975), Mar. Micropaleontol. 5 (1980) 321–325.

[15] D. Rio, I. Raffi, G. Villa, Pliocene–Pleistocene calcareous nannofossil distribution patterns in the western Mediterranean, Proc. Ocean Drill. Program Sci. Results 107 (1990) 513–533.

[16] J. Backman, N.J. Shackleton, Quantitative biochronology of Pliocene and Early Pleistocene calcareous nannoplankton from the Atlantic, Indian and Pacific Oceans, Mar. Micropaleontol. 8 (1983) 141–170.

[17] M.-P. Aubry, C. Requirand, J. Cook, The Rhomboaster–Tribrachiatus lineage: a remarkable succession of events from 55.5 to 53.2 Ma, GFF 122 (2000) 15–18.

[18] M.-P. Aubry, Provincialism in the photic zone during the LPTM, in: A. Ash, S. Wing (Eds.), Climate and Biota of the Early Paleogene, International Meeting, Powell, Wyoming, 2001, p. 6.

[19] M.-P. Aubry, K. Ouda, C. Dupuis, J.A. Van Couvering, the Members of the Working Group on the Paleocene/Eocene Boundary: J.R Ali, W.A. Berggren, H. Brinkhuis, P.R. Gingerich, C. Heilmann-Clausen, J. Hooker, D.V. Kent, C. King, R.W.B. Knox, P. Laga, E. Molina, B. Schimtz, E. Steurbaut, and D.R. Ward, Proposal: global standard stratotype-section and point (GSSP) at the Dababiya section (Egypt) for the base of the Eocene series, Int. Union Geol. Sc., Int. Comm. Strat., Subcomm. Paleogene Strat., 2002, 59 pp.

[20] A. Kahn, M.-P. Aubry, Provincialism associated with the Paleocene/Eocene Thermal Maximum: temporal constraint, Mar. Micropaleontol. 52 (2004) 117–131.

[21] I. Raffi, J. Backman, H. Pälike, Changes in calcareous nannofossil assemblage across the Paleocene/Eocene transition from the paleo-equatorial Pacific Ocean, Palaeogeogr. Palaeoclimatol. Palaeoecol. 226 (2005) 93–126.

[22] D. Bukry, Low-latitude coccolith biostratigraphic zonation, Initial Rep. Deep Sea Drill. Proj. 15 (1973) 685–703.

[23] M.-P. Aubry, B.S. Cramer, K.G. Miller, J.D Wright, D.V. Kent, R.K. Olsson, Late Paleocene event chronology: unconformities, not diachrony, Bull. Soc. Géol. France 171 (3) (2000) 367–378.

[24] K. Ouda, M.-P. Aubry, The Upper Paleocene–Lower Eocene of the Upper Nile Valley: Part 1. Stratigraphy, Micropaleontology, 49 (supplement 1), Micropaleontology Press, New York, NY, 2003, 212 pp.

[25] J. Backman, Late Paleocene to Middle Eocene calcareous nannofossil biochronology from the Shatsky Rise, Walvis Ridge and Italy, Palaeogeogr. Palaeoclimatol. Palaeoecol. 57 (1986) 43–59.

[26] S. Monechi, E. Angori, K. von Salis, Calcareous nannofossil turnover around the Paleocene/Eocene transition at Alamedilla (southern Spain), Bull. Soc. Geol. France 171 (4) (2000) 477–489.

[27] T.J. Bralower, Evidence of surface water oligotrophy during the Paleocene–Eocene Thermal Maximum: nannofossil assemblage data from Ocean Drilling Program Site 690, Maud Rise, Weddel Sea, Paleoceanography 17 (2) (2002) 1029–1042, doi:10.1029/2001PA000662.

[28] L.M. Bybell, J.M., Self trail, Evolutionary, biostratigraphic and taxonomic study of calcareous nannofossils from a continuous Paleocene–Eocene boundary section in New Jersey, Prof. Pap. - U.S. Geol. Survey 1554 (1995) (36 pp.).

[29] E. Angori, S. Monechi, High-resolution calcareous nannofossil biostratigraphy across the Paleocene–Eocene boundary at Caravaca (southern Spain), Israel J. Earth Sci. 44 (1996) 197–206.

[30] K. von Salis, S. Monechi, L.M. Bybell, J. Self-Trail, J. Young, Remarks on the calcareous nannofossil genera *Rhomboaster* and *Tribrachiatus* around the Paleocene/Eocene boundary, GFF 122 (2000) 138–140.

[31] A.J.T. Romein, Lineages in Early Paleogene calcareous nanno-plankton, Utrecht Micropaleont. Bull, Utrecht., vol. 22, 1979, 231 pp.

[32] W. Wei, S. Zhong, Taxonomy and magnetobiochronology of *Tribrachiathus bramlettei* and *Rhomboaster*, two genera of calcareous nannofossils, J. Paleontol. 70 (1) (1996) 7–22.

[33] M.-P. Aubry, Towards an Upper Paleocene–Lower Eocene high resolution stratigraphy based on calcareous nannofossil stratig-raphy, Israel J. Earth Sci. 44 (1996) 239–253.

[34] W. Wei, S.W. Wise Jr., Paleogene calcareous nannofossil mag-netochronology: result from South Atlantic DSDP Site 516, Mar. Micropaleontol. 14 (1989) 119–152.

[35] P.R. Bown, J.A. Lees, J.R. Young, Calcareous nannoplankton evolution and diversity through time, in: H.R. Thierstein, J.R. Young (Eds.), Coccolithophores—From Molecular Processes to Global Impact, Springer-Verlag, Berlin, 2004, pp. 481–508.

[36] M.-P. Aubry, From chronology to stratigraphy: interpreting the Lower and Middle Eocene stratigraphic record in the Atlantic Ocean, in: W.A. Berggren, et al., (Eds.), Geochronology, Time Scales and Global Stratigraphic Correlation, Soc. for Sediment. Geol., Tulsa, Okla., Spec. Publ., vol. 54, 1995, pp. 213–274.

[37] J.D.A. Zijderveld, A.C. demagnetization of rocks—analysis of results, in: D.W. Collinson, et al., (Eds.), Methods in Paleomag-netism, Elsevier, New York, NY, 1967, pp. 254–286.

[38] J.L. Kirschvink, The least-squares line and plane and the anal-ysis of palaeomagnetic data, Geophys. J. R. Astron. Soc. 62 (1980) 699–718.

[39] W. Lowrie, W. Alvarez, G. Napoleone, K. Perch-Nielsen, I. Premoli Silva, M. Toumarkine, Paleogene magnetic stratigraphy in Umbrian pelagic carbonate rocks: the Contessa sections, Gubbio, Geol. Soc. Amer. Bull. 93 (1982) 414–432.

[40] P.L. McFadden, M.W. McElhinny, Classification of the reversal test in palaeomagnetism, Geophys. J. Int. 103 (1990) 725–729.

[41] L. Tauxe, J. Besse, J.L. La Brecque, Palaeolatitudes from DSDP Leg 73 sediment cores; implications for the apparent polar wander path for Africa during the Late Mesozoic and Cenozoic, Geophys. J. R. Astron. Soc. 73 (1983) 315–324.

[42] D.A. Schneider, D.V. Kent, Testing models of the Tertiary pa-leomagnetic field, Earth Planet. Sci. Lett. 101 (1990) 260–271.

[43] C. Doglioni, A. Bosellini, Eoalpine and mesoalpine tectonics in the Southern Alps, Geol. Rundsch. 77 (1987) 734–754.

[44] M. Mattei, R. Funiciello, C. Kissel, Paleomagnetic and structural evidence for Neogene block rotations in the Central Apennines, Italy, J. Geophys. Res. 100 (B9) (1995) 17863–17883.

[45] G. Muttoni, D.V. Kent, E. Garzanti, P. Brack, N. Abrahamsen, M. Gaetani, Early Permian Pangea 'B' to Late Permian Pangea 'A', Earth Planet. Sci. Lett. 215 (2003) 379–394.

[46] G. Muttoni, D.V. Kent, E. Garzanti, P. Brack, N. Abrahamsen, M. Gaetani, Erratum to "Early Permian Pangea 'B' to Late Permian Pangea 'A': [Earth Planet Sci. Lett. 215 2003 379–394], Earth Planet. Sci. Lett. 218 (2004) 539–540.

[47] G. Rosenbaum, G.S. Lister, C. Duboz, The Mesozoic and Ceno-zoic motion of Adria (central Mediterranean): a review of con-straints and limitations, Geodin. Acta 17 (2) (2004) 125–139.

[48] J.E.T. Channell, Palaeomagnetism and palaeogeography of Adria, in: A. Morris, D.H. Tarling (Eds.), Palaeomagnetism and Tectonics of the Mediterranean Region, Geological Society Special Publication, London, 1996, pp. 119–132.

[49] W. Lowrie, W. Alvarez, Upper Cretaceous–Paleocene magnetic stratigraphy at Gubbio, Italy: III. Upper Cretaceous magnetic stratigraphy, Geol. Soc. Amer. Bull. 88 (1977) 374–377.

[50] D.V. Kent, P.E. Olsen, W.K. Witte, Late Triassic–earliest Juras-sic geomagnetic polarity sequence and paleolatitudes from drill cores in the Newark rift basin, eastern North America, J. Geo-phys. Res. 100 (1995) 14965–14998.

[51] G. Napoleone, I. Premoli Silva, F. Heller, P. Cheli, S. Corezzi, A.G. Fischer, Eocene magnetic stratigraphy at Gubbio, Italy, and its implications for Paleogene geochronology, Geol. Soc. Amer. Bull. 94 (1983) 181–191.

[52] S. Monechi, H.R. Thierstein, Late Cretaceous–Eocene nanno-fossil and magnetostratigraphic correlations near Gubbio, Italy, Mar. Micropaleontol. 9 (1985) 419–440.

[53] S.C. Cande, D.V. Kent, A new geomagnetic polarity time scale for the Late Cretaceous and Cenozoic, J. Geophys. Res. 97 (1992) 13917–13951.

[54] S.C. Cande, D.V. Kent, Revised calibration of the geomagnetic polarity time scale for the Late Cretaceous and Cenozoic, J. Geophys. Res. 100 (B4) (1995) 6093–6096, doi:10.1029/94JB03098.

[55] J. Backman, Quantitative calcareous nannofossil biochronology of Middle Eocene through Early Oligocene sediment from DSDP Sites 522 and 523, Abh. Geol. B.-A. 39 (1987) 21–31.

[56] J.P. Kennett, L.D. Stott, Abrupt deep-sea warming, paleoceano-graphic changes and benthic extinction at the end of the Paleo-cene, Nature 353 (1991) 225–229.

[57] U. Röhl, T.J. Bralower, R.D. Norris, G. Wefer, New chronology for the Late Paleocene Thermal Maximum and its environmental implications, Geology 28 (10) (2000) 927–930.

[58] G.R. Dickens, J.R. O'Neil, D.K. Rea, R.M. Owen, Dissociation of oceanic methane hydrate as a cause of the carbon isotope excursion at the end of the Paleocene, Paleoceanography 10 (1995) 965–971.

[59] A.C. Kurtz, L.R. Kump, M.A. Arthur, J.C. Zachos, A. Paytan, Early Cenozoic decoupling of the global carbon and sulfur cycles, Paleoceanography 18 (4) (2003) 1090, doi:10.1029/2003PA000908.

[60] H. Svensen, S. Planke, A. Malthe-Sørenssen, B. Jamtveit, R. Myklebust, T.R. Eidem, S.S. Rey, Release of methane from a volcanic basin as a mechanism for initial Eocene global warm-ing, Nature 429 (2004) 542–545.

[61] B.S. Cramer, D.V. Kent, Bolide summer: the Paleocene/Eocene Thermal Maximum as a response to an extraterrestrial trigger, Palaeogeogr. Palaeoclimatol. Palaeoecol. 224 (2005) 144–166.

[62] J.C. Zachos, M.W. Wara, S. Bohaty, M.L. Delaney, M.R. Pet-rizzo, A. Brill, T.J. Bralower, I. Premoli-Silva, A transient rise in tropical sea surface temperature during the Paleocene–Eocene Thermal Maximum, Science 302 (2003) 1551–1554.

[63] J.C. Zachos, U. Röhl, S.A. Schellenberg, A. Sluijs, D.A. Hodell, D.C. Kelly, E. Thomas, M. Nicolo, I. Raffi, L.J. Lourens, H. McCarren, D. Kroon, Rapid acidification of the ocean during the Paleocene–Eocene Thermal Maximum, Science 308 (2005) 1611–1615.

[64] U. Riesebell, I. Zondervan, B. Rost, P.D. Tortell, R.E. Zeebe, F.M.M. Morel, Reduced calcification of marine plankton in response to increased atmospheric CO_2, Nature 407 (2000) 364–367.

[65] W. Wei, S.W. Wise Jr., Middle Eocene to Pleistocene calcareous nannofossil recovered by Ocean Drilling Program Leg 113, in the Weddell Sea, Proc. Ocean Drill. Program, Sci. Results 113 (1990) 639–666.

[66] M.-P. Aubry, Late Paleogene calcareous nannoplankton evolution: a tale of climatic deterioration, in: D.R. Prothero, W.A. Berggren (Eds.), Eocene–Oligocene Climatic and Biotic Evolution, Princeton Univ. Press, Princeton, New Jersey, 1992, pp. 272–309.

[67] W.A. Beggren, D.V. Kent, J.J. Flynn, Paleogene geochronology and chronostratigraphy, in: N.J. Snelling (Ed.), The Chronology of the Geological Record, Mem. Geol. Soc. London, London, vol. 10, 1985, pp. 141–195.

[68] A. Boersma, I. Premoli Silva, Distribution of Paleogene planktonic foraminifera; analogies with the Recent? Palaeogeogr. Palaeoclimatol. Palaeoecol. 83 (1991) 29–48.

[69] P. Hallock, I. Premoli Silva, A. Boersma, Similarities between planktonic and larger foraminiferal evolutionary trends through Paleogene paleoceanographic changes, Palaeogeogr. Palaeoclimatol. Palaeoecol. 83 (1991) 49–64.

[70] P.D. Gingerich, Stratigraphic and micropaleontological constraints on the Middle Eocene age of the mammal-bearing Kuldana Formation of Pakistan, J. Vertebr. Paleontol. 23 (3) (2003) 643–651.

[71] K.D. Klitgord, H. Schouten, Plate kinematics of the central Atlantic, in: B.E. Tucholke, P.R. Vogt (Eds.), The Geology of North America, The Western North Atlantic Region, Geol. Soc. of Am. Boulder, CO, 1986, pp. 351–378.

[72] S.P. Srivastava, C.R. Tapscott, Plate kinematics of the North Atlantic, in: B.E. Tucholke, P.R. Vogt (Eds.), The Geology of North America, The Western North Atlantic Region, Geol. Soc. of Am. Boulder, CO, 1986, pp. 379–404.

[73] J. Besse, V. Courtillot, Apparent and true polar wander and the geometry of the geomagnetic field in the last 200 million years, J. Geophys. Res. 107 (B11) (2002) 2300, doi:10.1029/2000JB000050.

[74] J. Besse, V. Courtillot, Correction to "Apparent and true polar wander and the geometry of the geomagnetic field over the last 200 Myr", J. Geophys. Res. 108 (B10) (2003) 2469, doi:10.1029/2003JB002684.